Appl Phys A (2014) 114:847–852
DOI 10.1007/s00339-013-7704-5

Applied Physics A
Materials Science & Processing

Effect of cation and anion defects on the resistive switching polarity of ZnO_x thin films

Xinghui Wu · Zhimou Xu · Binbing Liu · Tangyou Sun · Wenning Zhao · Sisi Liu · Zhichao Ma · Fei Zhao · Shuangbao Wang · Xueming Zhang · Shiyuan Liu · Jing Peng

Received: 16 January 2013 / Accepted: 9 April 2013 / Published online: 25 April 2013
© Springer-Verlag Berlin Heidelberg 2013

Abstract In this paper, we achieve the resistive switching (RS) polarity from unipolar to bipolar in a simple Al/ZnO_x/Al structure by moderating the oxygen content in the ZnO sputtering process. In a pure Ar sputtering, Al/ZnO_x/Al shows unipolar behavior, as oxygen partial pressure increases, the RS polarity changes to bipolar, and the switch current decreases by about five orders of magnitude. The current transport properties of unipolar device show ohmic behavior under both high resistance (HRS) and low resistance states (LRS), but the bipolar device shows Schottky barrier modulated current transport properties. We study the defect types in the unipolar and bipolar devices through photoluminescence (PL) spectra. The PL results show that the interstitial zinc (Zn_i) and interstitial oxygen (O_i) are dominant in unipolar and bipolar devices, respectively. We attribute this phenomenon to Zn_i and O_i playing important role in unipolar (URS) and bipolar resistive switching (BRS), respectively.

The authors declare no competing financial interest.

X. Wu · Z. Xu (✉) · B. Liu · T. Sun · W. Zhao · S. Liu · Z. Ma · F. Zhao · S. Wang · X. Zhang
Wuhan National Laboratory for Optoelectronics, School of Optical and Electronic Information, Huazhong University of Science and Technology, 430074 Wuhan, People's Republic of China
e-mail: xuzhimou@mail.hust.edu.cn

S. Liu
School of Mechanical Science and Engineering, Huazhong University of Science and Technology, 430074 Wuhan, People's Republic of China

J. Peng
College of Sciences, Wuhan University of Science and Technology, 430081 Wuhan, People's Republic of China

Abbreviations

RS	Resistive switching
URS	Unipolar resistive switching
BRS	Bipolar resistive switching
HRS	High resistance state
LRS	Low resistance state
Zn_i	Interstitial zinc
O_i	Interstitial oxygen
V_O	Oxygen vacancy
V_{Zn}	Zn vacancy
XRD	X-ray diffraction
SEM	Scanning electron microscopy
PL	Photoluminescence
SCLC	Space charge limited conduction
SCCM	Standard-state cubic centimeter per minute

1 Introduction

The resistive switching phenomenon at simple metal–semiconductor–metal junctions has attracted much attention due to not only fundamental interest in the mechanisms but also the potential uses in next-generation nonvolatile memory devices. Several properties caused the researchers' interest, such as conduction mechanism, cell endurance, switching speed and memory density. Among these crucial parameters, the memristor polarity is an important issue that has attracted interest of many researchers. According to whether it depends on the operating voltage polarity, the RS polarity can be classified into two types: unipolar (URS) and bipolar resistive switching (BRS) [1].

So far, for the same kind of materials even with different preparation methods, the resistance switching polarities are not identical. Such are binary metal oxides: NiO [2, 3],

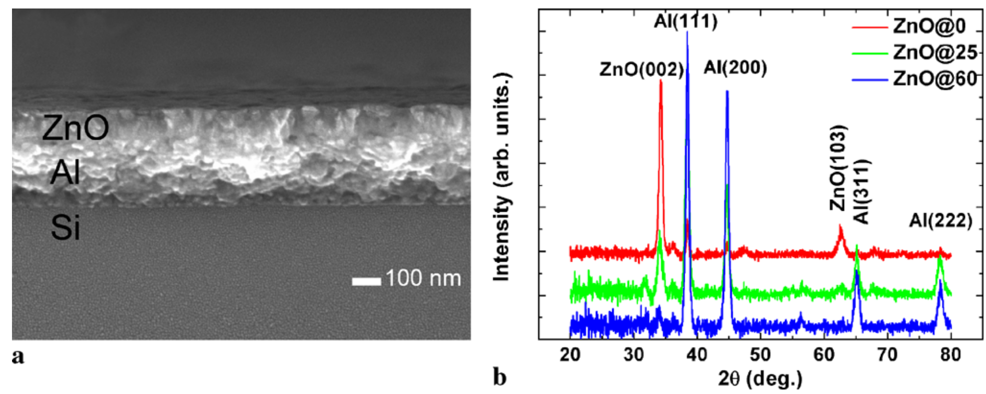

Fig. 1 (**a**) The cross section image of ZnO@0/Al/Si structure. (**b**) The XRD pattern of three types of ZnO films sputterings grown on Al/Si substrate

TiO_2 [4, 5], ZnO [6, 7], TaO_x [8, 9]. We know that different material preparation methods may cause different type defects, metal interstitial-type defect or oxygen vacancy defect, which would affect the device switching polarity.

Previous studies have shown coexistence of BRS and URS in several metal-oxide-based memory cells. Goux et al. showed that the two switching modes can be activated by using an optimized oxidation process (1 min) of a Ni blanket layer. Short oxidation (30 s) resulted in shortcut cell, while long oxidation (≫1 min) resulted in common URS [10]. The two switching modes also can be changed in pure Ar sputtering ZnO based thin films [11], but the resistive switching mode commonly displays bipolar deposit in mixed Ar and O_2 working gas [12]. Lee et al. [13] and Sun et al. [14] reported resistive switching change between the BRS and URS in $SrTiO_3$, and the studies indicate the importance of defect control engineering in RS. In addition, there were similar reports about TiO_2 [15] and HfO_2 [16] based RS phenomenon. Recent study has shown the conversion from unipolar to bipolar resistance switching by inserting a stoichiometric Ta_2O_5 layer in Pt/TaO_x/Pt cells [8]. Oka et al.'s recent studies demonstrated that coexistence of anion and cation defects is critical to the transport properties of p-type NiO [17]. So the defects and stoichiometry in the active switching region would have an important influence on electrical transport and RS polarity.

In this study, we showed the effects of cation and anion defects and the device interfacial characteristic on the RS polarity. We studied the RS behavior which can be modulated by changing cation and anion defects concentration during deposition of ZnO thin films. URS mode devices were observed in pure Ar sputtering; interestingly, with increasing oxygen partial pressure, the devices cells show BRS feature. The PL spectra results show that the Zn_i/O_i ratio decreases with increased oxygen content. From these results, a model is discussed to explain these systematic changes.

2 Experimental

The resistive switching structure, having a metal–semiconductor–metal layout, was prepared by depositing Al, ZnO, Al in sequence on P–Si substrate. Initially, 250-nm thick Al films were deposited on P–Si by DC magnetron sputtering. Subsequently, ZnO films were added by reactive RF magnetron using a 10 cm diameter by 0.8 cm thick ZnO target (99.99 %) at room temperature in different oxygen partial pressure. The oxygen partial pressure is defined as $PO_2\ (\%) = p(O_2)/p(Ar + O_2)$. The working pressure was maintained at about 0.33 Pa. The resistive switching in ZnO films with oxygen partial pressure of 0, 25 and 60 % obtained with various O_2 flow rates during deposition are hereafter respectively denoted as ZnO@0, ZnO@25 and ZnO@60. For electrical measurement, circuit Al top electrodes (200 nm thick, 200 µm in diameter) were deposited on ZnO films by sputtering using a metal shadow mask. All fabrication process was carried out at room temperature and no post-processing was used.

The microstructure and crystal structure were examined by scanning electron microscopy (SEM, JSM-7600F) and X-ray diffraction (XRD, PANalytical PW3040/60). The film thickness was observed by SEM and generalized ellipsometer (developed by Huazhong University of Science and Technology). The presence and types of oxygen- and zinc-related defects were investigated by photoluminescence (PL, FP-6500) spectroscopy using the 325-nm line of He–Cd laser as the excitation source. The I–V curves of memory cell were measured by semiconductor characteristic measurement system (Keithley 4200 SCS) at room temperature in ambient condition. The measurements were performed by a DC voltage sweep mode and all the bias voltages were applied on top electrode with bottom electrode grounded.

3 Results and discussion

Figure 1(a) shows the SEM image of ZnO@0 Al/Si cross section of the structure. The result shows that the ZnO films

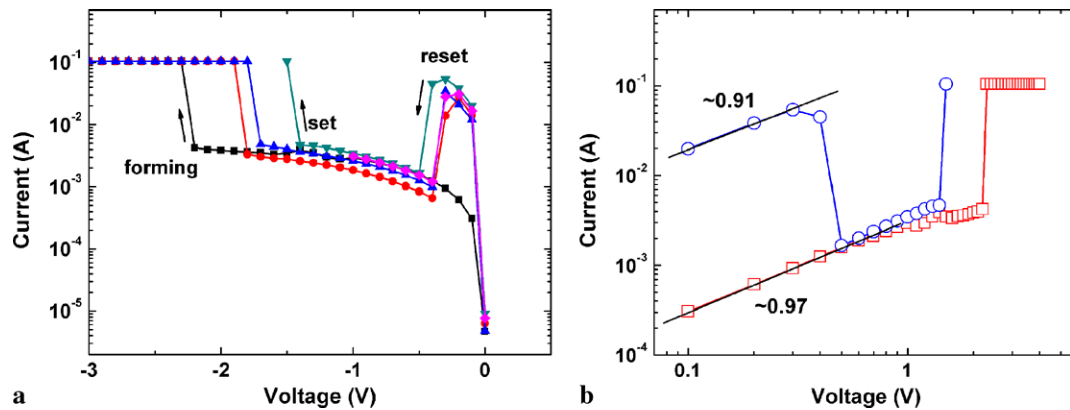

Fig. 2 (**a**) Typical I–V characteristic of URS in Al/ZnO@0/Al cell. (**b**) I–V characteristic in a double-logarithmic scale. The different values of slope are listed in the plots

have a columnar grain structure to the substrate. It suggests that the ZnO preferential growth direction is along (002). It can be found that the thickness of ZnO and Al bottom electrode was about 120 and 250 nm, respectively. The film thickness of ZnO@25 and ZnO@60 confirmed by generalized ellipsometer was 60 and 40 nm, respectively. And the deposition rate of ZnO@0, ZnO@25 and ZnO@60 was 8.6, 4 and 3.5 nm/min respectively, according to the deposition time.

The XRD pattern of ZnO films deposited on Al/Si substrate is shown in Fig. 1(b). It shows that the ZnO films exhibit polycrystalline properties, and have a c-axis preferred orientation, in agreement with SEM result. It was also found that with increase in film thickness, the (002) peaks intensity becomes larger. It indicates the improved ZnO crystalline properties.

Figure 2(a) shows the I–V curve of the memory device ZnO@0. The device displays unipolar resistance switching behavior. The I–V curves are systematic with respect to the polarity of the bias voltages. To prevent permanent damage during the forming and setting processes, the current flow was limited by a compliance current [8]. For simplicity, we show the negative voltage side only.

When −3 V voltage was applied to the pristine cell, it was observed that, with increase of the applied voltage from 0 to −3 V, the device was originally in the HRS and a setting process occurred at about −2.2 V (V_{set}).

When again −3 V bias was applied to the device, the LRS returned to a high-resistance state (HRS) at 0.3 V. The URS setting process usually is known to originate from the conduction filament formed by mobile metal ions under electric field. The reset process originated from filamentary rupture controlled by Joule heating, and shows no polarity dependence [2, 7]. Zn_i and oxygen vacancy (V_O) are generally considered to be the main reasons causing unintentional n-type conductivity of ZnO [18]. So the URS characteristic of the Al/ZnO@0/Al cell may come from the Zn_i and V_O related defects.

In order to investigate the origin of the switching characteristic of the device, the I–V curves were re-plotted in double-logarithmic scale, as shown in Fig. 2(b). It can be seen that under HRS and LRS in the voltage sweep region, the I–V curves show linear behavior; this suggests that the I–V characteristic follows the Ohm's law and is regarded as the charge transport of a conductor system. And it also indicates that the interface contact shows ohmic contact.

Figure 3(a) representatively shows voltage sweeps programming the cell of ZnO@25 under different compliance currents. It can be found that the resistive switching polarity shows a typical BRS characteristic. The device is originally in the HRS; with increasing the applied voltage the current of the device increased slowly and the setting voltage became about 3 V. Afterwards, by sweeping the voltage to a negative value, the current decreased and the state of the device switched again to HRS. In order to characterize the effect of the compliance current on the RS polarity, we studied the I–V properties of the memory cell under four different compliance current settings: 90, 400, 600 and 900 µA. It can be seen that the cell is showing a stable BRS behavior.

Both positive and negative sweeps are shown in Fig. 3(b) in double-logarithmic scale. From the positive voltage sweep plot we can see that in the low voltage range ($0 \to 0.5$ V) the I–V characteristic first exhibits linear properties and then shows quadratic characteristic with the slope ~ 2.08. With further increasing the applied voltage ($2.5\ \text{V} < V_{applied} < 3\ \text{V}$), the current rises rapidly and the slope reaches 6–8. The current transport characteristic in the device can be explained by a trap-controlled space charge limited conduction (SCLC) mechanism [19, 20].

Figure 4(a) shows the I–V curve of a sample ZnO@60 in semi-logarithmic scale. Obviously, the resistive switching polarity also shows BRS. The numbered arrows indicate the voltage sweep direction. Clearly, nonlinear and cutoff properties of HRS current characteristic indicate that

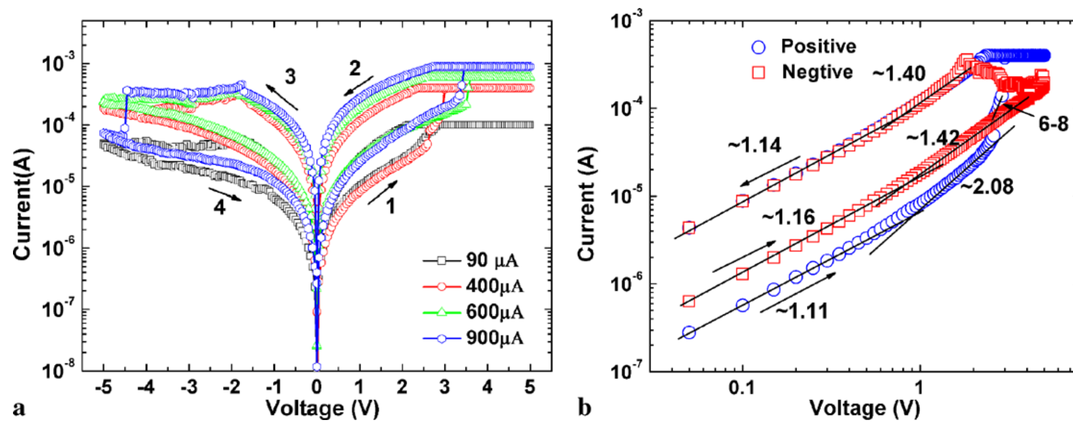

Fig. 3 (**a**) I–V curves of resistive switching loops at different compliance currents of Al/ZnO@25/Al cell. The *numbered arrows* indicate the voltage sweep direction. (**b**) I–V characteristic in a double-logarithmic scale, the different values of slopes listed in the plots. *Arrow* shows the voltage sweep direction

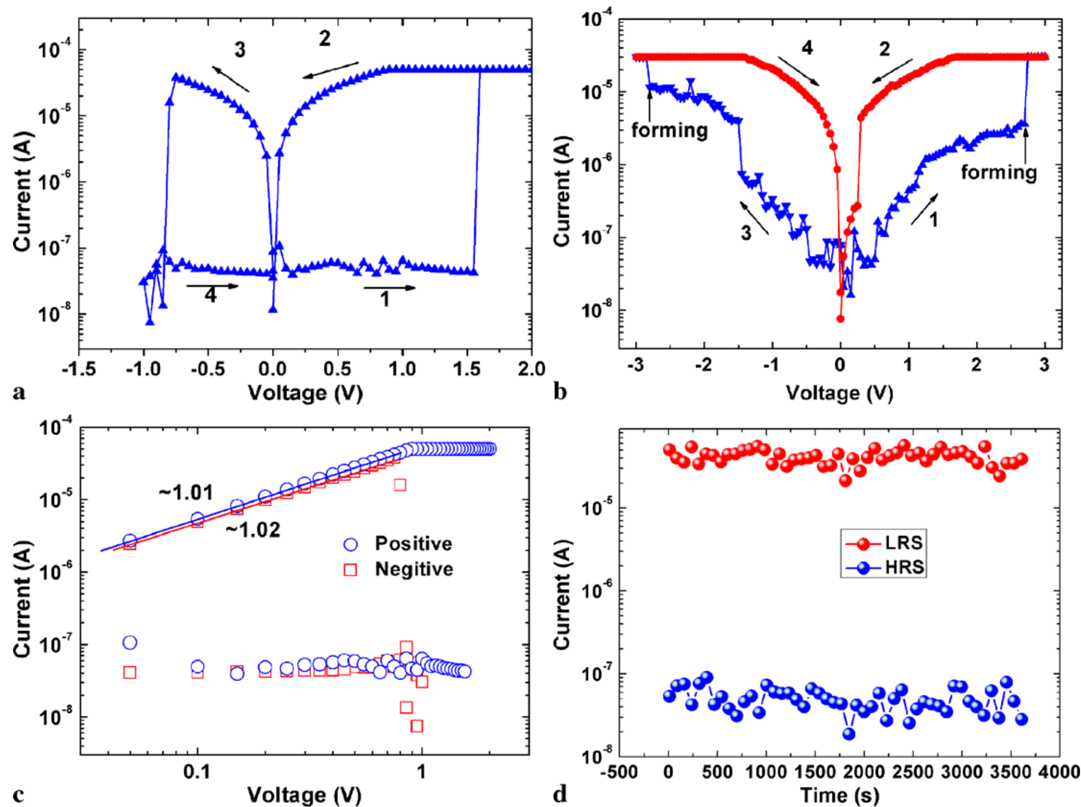

Fig. 4 (**a**) I–V curve of Al/ZnO@60/Al cell showing BRS characteristic. (**b**) The forming process of the cell. (**c**) The voltage sweep I–V curve in a double-logarithmic scale. (**d**) Retention data of the Al/ZnO@60/Al device at room temperature

the ZnO makes Schottky barrier with bottom and top electrodes. Figure 4(b) shows the cell forming process. The voltage sweep direction is 0 V → +3 V → 0 V, and then 0 V → −3 V → 0 V. It can be seen that in the initial state both the positive and negative voltage directions show high resistance. Figure 4(c) shows the same I–V curve data in double-logarithmic scale. The I–V characteristic appears linear under LRS. The slope in positive and negative voltage directions is about 1.01 and 1.02, respectively. This phenomenon indicates that the Schottky barrier disappeared and the interface contact transformed into ohmic contact after a setting process. The device retention (bias at 0.75 V) performance for both resistance states is as displayed in Fig. 4(d). It shows that both states are stable within 3600 s.

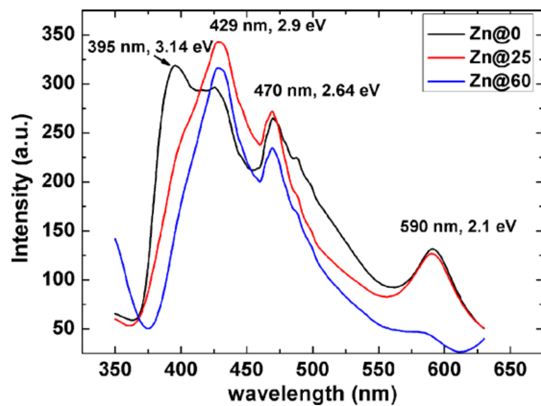

Fig. 5 Room temperature PL spectra of ZnO films prepared at various oxygen contents

According to the metal/semiconductor contact theory, the Schottky barrier should be neglected at the Al/ZnO interface due to the work function value of Al (~4.28 eV), ZnO (~4.1 eV) [21]. But the interface contact and conduction mechanism for the three devices are obviously different. The ZnO@60 cell shows Schottky contact with electrodes, while the ZnO@0 cell shows ohmic contact, and the ZnO@25 cell shows SCLC mode charged transport. The standard Gibbs free energy of formation of Al oxide is −1582.3 kJ/mol, which is far lower than of the ZnO (−320.5 kJ/mol). Al electrode can get O^{2-} from ZnO and form AlO_x, so the following reaction occurs: $Al + O^{2-} \rightarrow AlO_x$ [22]. And the interfacial oxide layer was confirmed by other studies in the image of TEM [12, 23] or AES [24]. Therefore the AlO_x acts as a barrier layer blocking the current transport, so the HRS of ZnO@60 shows the Schottky contact characteristic, and the original I–V curve at both positive and negative voltages shows cut-off behavior. But to ZnO@0 cell there is not enough thickness of oxide barrier layer at the interface to block the charge transport, the device acts as a conductor in the circuit, so the current shows linear behavior no mater whether before or after the switching. The SCLC type shown in ZnO@25 is intermediate state between Schottky contact and ohmic contact.

To investigate the types of the defect on the resistive switching behavior, PL spectra of ZnO/Al/Si films were carried out at room temperature, and the results are shown in Fig. 5. Four emission peaks at 395 nm (3.14 eV), 429 nm (2.9 eV), 470 nm (2.64 eV), and 590 nm (2.1 eV) are found in the three types of samples. On the basis of previous studies, these peaks related to several types of intrinsic defects in the ZnO growth, such Zn_i, Zn vacancy (V_{Zn}), V_O and O_i [18, 25].

The 395 nm emission is originally from band transition from Zn_i level to valence band according to the full potential linear muffin-tin orbital method [26]. The curve shows that with the oxygen content increase the intensity of 395 nm emission peak decreases, and the content of Zn_i decreases with the oxygen partial pressure increase.

The 429 nm (2.9 eV) emission peak is due to the O_i related defects. Previous studies show that the O_i lie 2.96 eV from the conduction band in ZnO; they suggest that the 429 nm emission comes from radiation from the conduction band to O_i level [27, 28]. Ahn et al. suggested that ZnO films grown at O_2 flow rates of 50 standard-state cubic centimeters per minute (SCCM) showed blue emission at 2.85 eV by MOCVD at room temperature, but corresponding emission not found at 10 SCCM [29]. They claimed that during ZnO growth process using excess oxygen gas leads to formation of oxygen interstitial sites. So we consider the 429 nm emission peak associated with O_i related defect. It has been shown that the intensity of 470 nm emission peaks enhanced with O_2 partial pressure decreased in Ar/O_2 atmosphere RF sputtering ZnO films [30], which would account for V_O to the 470 nm emission peak.

Previous studies indicated that the 590 nm (2.1 eV) emission is related to V_OZn_i complex in the films [31], the calculation predicted the energy of complex V_OZn_i lying 2.16 eV below the conduction band minimum [32]. They found that the 590 nm emission peak disappeared in the 60 % oxygen partial pressure. Since with oxygen content increased the concentration of both V_O and Zn_i defects decreased subsequently, the concentration of complex V_OZn_i may have become very low, and resulting 590 nm emission disappeared.

We also observed that the HRS resistance in the three devices was 3.4×10^2, 1.22×10^5 and 1.57×10^7 Ω at 1 V for respective sample ZnO@0, ZnO@25 and ZnO@60. This means that the switch current of the device decreased with oxygen partial pressure. This reason mainly is that the acceptor O_i can compensate for the electronic carrier formed by V_O and Zn_i, thus reducing the film conductivity. And these non-lattice oxygen ions also play important role in resistance switching process, which would drift to electrode under the applied bias voltage and redox reaction occurring at the interface. We know that the low switching current is important in nanoscale size memory, as the µA-scale switch current is favorable in designing nanoscale RRAM [33].

From the PL results we also observed that the relative intensity of 395 to 429 nm emission peaks decreased with oxygen partial pressure, thereby suggesting that Zn_i defect density decreased with oxygen partial, while O_i density increased with oxygen partial, and the relative quantity of Zn_i to O_i increased at room temperature sputtering.

Based on the above analysis, we assumed the following mechanism for URS and BRS. For the URS, when a negative bias is applied to the top electrode, the Zn^+ drifts under strong electronic field gathering tiny conducting filaments, resulting in low resistance state. Subsequently, when applying to it the same polarity voltage, the cell returned to HRS due to Joule heating enhanced filaments oxidation.

For the BRS, the cell resistance was mainly controlled by naturally formed Schottky barrier junction at the interface. The resistive switching comes from AlO_x barrier layer formation and reduction. After the forming process, the device is in LRS and the I–V curve characteristic shows linear behavior: at this time the Schottky barrier is disappearing. When negative voltage is applied to the top electrode, O^{2-} moves to the bottom electrode resulting in redox action of AlO_x layer as insulated layer. Due to the barrier, I–V curve displays a cut-off characteristic in the HRS. When the positive voltage is applied to the top electrode, the following reduction reaction occurs: $AlO_x \rightarrow Al + O^{2-}$, resulting in LRS.

4 Conclusions

In conclusion, we studied the effect of cation and anion defects on the RS polarity based on Al/ZnO_x/Al memristive device. By modulating the oxygen partial pressure, we can change the resistive switching polarity from URS to BRS. In low oxygen content, the device shows URS, the current transport follows ohmic law, while with increasing oxygen content, the device shows BRS, and the electron transport displays a Schottky barrier modified characteristic. The PL spectra data indicate that the concentration of Zn_i and O_i defects was obviously different in URS and BRS devices. The URS behavior attributes to the Zn_i formed filament and rupture. While the BRS behavior attributes to the reverted AlO_x formed by O^{2-} and the electrode at interface. The presented results suggest that defects of anion and cation play an important role in resistive switching behavior.

Acknowledgements This work was supported by the National Natural Science Foundation of China (Grant Nos. 61076042 and 60607006); the Special Project on Development of National Key Scientific Instruments and Equipment of China (Grant No. 2011YQ16000205), and National Key Technology RD Program of China (Grant No. 2009BAH49B01).

References

1. R. Waser, R. Dittmann, G. Staikov, K. Szot, Adv. Mater. **21**, 2632 (2009)
2. M.-J. Lee, S. Han, S.H. Jeon, B.H. Park, B.S. Kang, S.-E. Ahn, K.H. Kim, C.B. Lee, C.J. Kim, I.-K. Yoo, D.H. Seo, X.-S. Li, J.-B. Park, J.-H. Lee, Y. Park, Nano Lett. **9**, 1476 (2009)
3. J. Sullaphen, K. Bogle, X. Cheng, J.M. Gregg, N. Valanoor, Appl. Phys. Lett. **100**, 203155 (2012)
4. J.J. Yang, M.D. Pickett, X.M. Li, D.A.A. Ohlberg, D.R. Stewart, R.S. Williams, Nat. Nanotechnol. **3**, 429 (2008)
5. D.H. Kwon, K.M. Kim, J.H. Jang, J.M. Jeon, M.H. Lee, G.H. Kim, X.-S. Li, G.-S. Park, B. Lee, S. Han, M. Kim, C.S. Hwang, Nat. Nanotechnol. **5**, 148 (2010)
6. Y.C. Yang, F. Pan, Q. Liu, M. Liu, F. Zeng, Nano Lett. **9**, 1636 (2009)
7. W.Y. Chang, Y.C. Lai, T.B. Wu, S.F. Wang, F. Chen, M.J. Tsai, Appl. Phys. Lett. **92**, 022110 (2008)
8. H.K. Yoo, S.B. Lee, J.S. Lee, S.H. Chang, M.J. Yoon, Y.S. Kim, B.S. Kang, M.J. Lee, C.J. Kim, B. Kahng, T.W. Noh, Appl. Phys. Lett. **98**, 183507 (2011)
9. C. Chen, C. Song, J. Yang, F. Zeng, F. Pan, Appl. Phys. Lett. **100**, 253509 (2012)
10. L. Goux, J.G. Lisoni, M. Jurczak, D.J. Wouters, L. Courtade, C. Muller, J. Appl. Phys. **107**, 024512 (2010)
11. S. Lee, H. Kim, J. Park, K. Yong, J. Appl. Phys. **108**, 076101 (2010)
12. C. Chen, F. Pan, Z.S. Wang, J. Yang, F. Zeng, J. Appl. Phys. **111**, 013702 (2012)
13. S.B. Lee, J.S. Lee, S.H. Chang, H.K. Yoo, B.S. Kang, B. Kahng, M.J. Lee, C.J. Kim, T.W. Noh, Appl. Phys. Lett. **98**, 033502 (2011)
14. X. Sun, G. Li, X. Zhang, L. Ding, W. Zhang, J. Phys. D, Appl. Phys. **44**, 125404 (2011)
15. D.S. Jeong, H. Schroeder, R. Waser, Electrochem. Solid-State Lett. **10**, G51 (2007)
16. L. Goux, Y.Y. Chen, L. Pantisano, X.P. Wang, G. Groeseneken, M. Jurczak, D.J. Wouters, Electrochem. Solid-State Lett. **13**, G54 (2010)
17. K. Oka, T. Yanagida, K. Nagashima, M. Kanai, B. Xu, B.H. Park, H. Katayama-Yoshida, T. Kawai, J. Am. Chem. Soc. **134**, 2535 (2012)
18. A. Janotti, C.G. Van de Walle, Phys. Rev. B **76**, 165202 (2007)
19. Q. Wang, D.S. Shang, Z.H. Wu, L.D. Chen, X.M. Li, Appl. Phys. A, Mater. Sci. Process. **86**, 357 (2006)
20. D.S. Shang, Q. Wang, L.D. Chen, R. Dong, X.M. Li, W.Q. Zhang, Phys. Rev. B **73**, 245427 (2006)
21. E.H. Rhoderick, R.H. Williams, *Metal–Semiconductor Contact* (Oxford University Press, Oxford, 1988)
22. R.L. David, *CRC Handbook of Chemistry and Physics*, 77th edn. (CRC, Boca Raton, 1996–1997)
23. H.Y. Jeong, J.Y. Lee, S.-Y. Choi, Appl. Phys. Lett. **97**, 042109 (2010)
24. R. Yang, X.M. Li, W.D. Yu, X.D. Gao, D.S. Shang, X.J. Liu, X. Cao, Q. Wang, L.D. Chen, Appl. Phys. Lett. **95**, 072105 (2009)
25. Y.W. Heo, D.P. Norton, S.J. Pearton, J. Appl. Phys. **98**, 073502 (2005)
26. H. Zeng, Z. Gang, W. Cai, P. Liu, J. Appl. Phys. **102**, 104307 (2007)
27. K.H. Tam, C.K. Cheung, Y.H. Leung, A.B. Djurišić, C.C. Ling, C.D. Beling, S. Fung, W.M. Kwok, W.K. Chan, D.L. Phillips, L. Ding, W.K. Ge, J. Phys. Chem. B **110**, 20865 (2006)
28. Z. Fu, B. Lin, G. Liao, Z. Wu, J. Cryst. Growth **193**, 316 (1998)
29. C.H. Ahn, Y.Y. Kim, D.C. Kim, S.K. Mohanta, H.K. Cho, J. Appl. Phys. **105**, 013502 (2009)
30. K.K. Kim, J.H. Song, H.J. Jung, W.K. Choi, S.J. Park, J.Y. Lee, J. Vac. Sci. Technol. A **18**, 2864 (2000)
31. S.-H. Jeong, B.-S. Kim, B.-T. Lee, Appl. Phys. Lett. **82**, 2625 (2003)
32. P.S. Xu, Y.M. Sun, C.S. Shi, F.Q. Xu, H.B. Pan, Nucl. Instrum. Methods Phys. Res., Sect. B, Beam Interact. Mater. Atoms **199**, 286 (2003)
33. M.J. Lee, C.B. Lee, D. Lee, S.R. Lee, M. Chang, J.H. Hur, Y.B. Kim, C.J. Kim, D.H. Seo, S. Seo, U.I. Chung, I.K. Yoo, K. Kim, Nat. Mater. **10**, 625 (2011)